symmetry

MDPI

Article

Influence of Elastic–Plastic Deformation on the Structure and Magnetic Characteristics of 13Cr-V Alloyed Steel Pipe

Evgeniia Putilova * and Kristina Kryucheva

Institute of Engineering Science, Ural Branch of the Russian Academy of Sciences (IES UB RAS), 620078 Ekaterinburg, Russia; kristina.kryucheva@mail.ru

* Correspondence: tuevaevgenya@mail.ru; Tel.: +792-2111-3637

Abstract: The principle of symmetry is one of the general methodological principles of science. The effects of any external influences, such as deformation, stresses, temperature, etc., could lead to the anisotropy (asymmetry) of properties in constructional materials. During operation, metal structures and machine parts are exposed to time-varying external mechanical loads, which can cause changes in the metal structure, the initiation of cracks, and, as a result, the destruction of the product. The application of nondestructive testing methods prevents changes in the stress–strain state and, consequently, the destruction of the object. This article contains the results of studying the effects of elastic–plastic deformation by uniaxial tension and torsion on the change in the structure and magnetic parameters of low-alloy 13Cr-V pipe steel. Modern methods of metallography and magnetic nondestructive testing methods were used as part of this study. The results of the EBSD analysis showed that deformation during torsion, in contrast to uniaxial tension, is unevenly distributed over the sample cross section. In the cross section of the sample, the most severely deformed grains with a change in their geometry are observed near the surface; in the center, there is no change in geometry. During tension, the deformation over the cross section of the sample is uniformly distributed. Correlations between the applied normal and tangential stresses and magnetic characteristics of the 13Cr-V structural steel were determined. Informative parameters that could be used for the development of nondestructive testing methodologies for solving concrete tasks were determined. Different methods of deformation lead to diverse structural changes in grain structure.

Keywords: elastic and plastic deformation; tension; torsion; magnetic properties; stress–strain state; coercive force; residual induction; maximum magnetic permeability

Citation: Putilova, E.; Kryucheva, K. Influence of Elastic–Plastic Deformation on the Structure and Magnetic Characteristics of 13Cr-V Alloyed Steel Pipe. *Symmetry* **2022**, *14*, 1201. https://doi.org/10.3390/sym14061201

Academic Editor: Zine El Abiddine Fellah

Received: 5 May 2022
Accepted: 6 June 2022
Published: 10 June 2022

1. Introduction

Metal structures and machine parts are subjected to time-varying external mechanical loads during operation, which can cause changes in the structure of the metal and the accumulation of microdefects, and, consequently, the formation of macrodefects, the initiation of cracks, and, as a result, the destruction of the object. Despite the development and active introduction of modern materials (composite, metal-ceramic, etc.), the use of steels and alloys as the main material for critical metal structures is still widespread, especially in the railway industry [1,2], the pipeline and oil and gas industries [3–5], heavy engineering [6], etc. Severe operating conditions of such facilities could lead not only to material losses, but also, in certain situations, to a negative impact on the environment and the death of people. Information about the existing stresses makes it possible to take preventive measures, e.g., to strengthen the dangerous zone, or to remove the stresses by making changes to the elements of the existing structure.

Along with standardized methods for assessing the stress–strain state (tensometric, acoustic and X-ray), interest is also shown in magnetic methods for monitoring the stress–strain state of steel structures. A sufficient amount of work has been devoted to the application of the Barkhausen magnetic noise method for assessing the stress–strain state

of steel objects [7–11]. Some work has been devoted to evaluating the level of residual stress in metallic materials [7], while other work provides data on the possibilities of assessing applied stresses [8,10,11], including those under biaxial loading [9]. The use of electromagnetic methods based on the measurement of magnetic incremental permeability and magnetic flux leakage [12,13] and ultrasonic methods [13] also allows one to estimate the level of applied stresses. However, the use of magnetic methods is not always possible, and often has a limited range of applicability [14]. Some work shows such limitations and the possible solutions, including the use of several techniques simultaneously [12,15,16]. In general, we can say that the application of magnetic methods is based on the correlations between the mechanical and magnetic characteristics of structural materials.

In the field of nondestructive testing, the study of magnetoelastic phenomena in structural ferromagnetic materials makes it possible to make progress in the issue of estimating the parameters of the stress–strain state of individual structural elements. As a consequence, the use of these parameters in modelling representations of the mechanics of deformation and fracture mechanics will allow the development of a methodology for assessing the state and resourcefulness of individual elements and the structure as a whole.

It should also be noted that any changes in physical, including magnetic, parameters are determined by changes occurring in the structure of the material (grain, dislocation, etc.), as well as a change in the level of residual stress in the material [17,18] under external deformation action. So, for example, the chemical composition of steel has a significant effect on the magnetic parameters, since varying the content of alloying elements in steel could lead to a change in the grain (for example, the formation of a reinforced structure, which, in turn, leads to an increase in the values of the coercive force [19,20]), dislocation (dislocations and their clusters impede the movement of domain walls and, hence, the process of magnetization [21]) of the structure, as well as to the transition of steel from one class to another (from purely austenitic to austenitic-ferritic, for example [22]). The analyses of magnetic parameters' behavior and their symmetry (or asymmetry) distributions could contribute to that of the stress–strain state parameters of the investigated material.

Despite the large number of existing publications, the results of which can be used to create physical nondestructive methods for diagnosing the current state of structural materials and assessing their resourcefulness, this problem has not yet been completely solved and remains relevant. In addition, each specific object made of a particular steel, or a group of objects with similar operating conditions, requires a more detailed study. This article contains the results of studying the effect of elastic–plastic deformation by uniaxial tension and torsion on the change in the structure and magnetic parameters of low-alloy 13Cr-Vsteelpipe. Ensuring the safe operation of critical facilities, such as pipelines operating under pressure, makes the problem of performing a reliable assessment of their current stress–strain state more relevant. In this work, an experiment was implemented that makes it possible to simulate the effect of both normal and shear stresses on the change in magnetic characteristics. Moreover, it was possible to carry out measurements of the magnetic parameters in situ. No such studies have been carried out for 13Cr-V-grade steel.

2. Materials and Methods

The studies were carried out on cylindrical samples cut from 13Cr-V steel pipe, the chemical composition of which is given in Table 1.

Table 1. Chemical composition of the steel under investigation, wt. %.

C	Si	Mn	Cr	Ni	Mo	Cu	V	P	S
0.04	0.31	0.65	0.56	0.09	0.01	0.15	0.06	0.006	0.002

Mechanical tests of uniaxial tension and torsion were carried out on the samples at room temperature using universal testing equipment, created on the basis of IES UB RAS, until the sample ruptured. The maximum allowable tensile force was 50 kN and

the maximum torque was 200 N·m. The appearance and layout of the setup are shown in Figure 1a,b. The setup also allows for internal pressure tests, but no such studies were carried out in this work. The type of investigated sample is shown in Figure 1c. This type of sample was used for both tension and torsion. The working part of the sample, where the deformation took place, was under the action of an electromagnet. The measuring coil was placed in the middle of the working part. At least three samples were used for each type of loading. The error in the measured values of the magnetic parameters was no more than 7%.

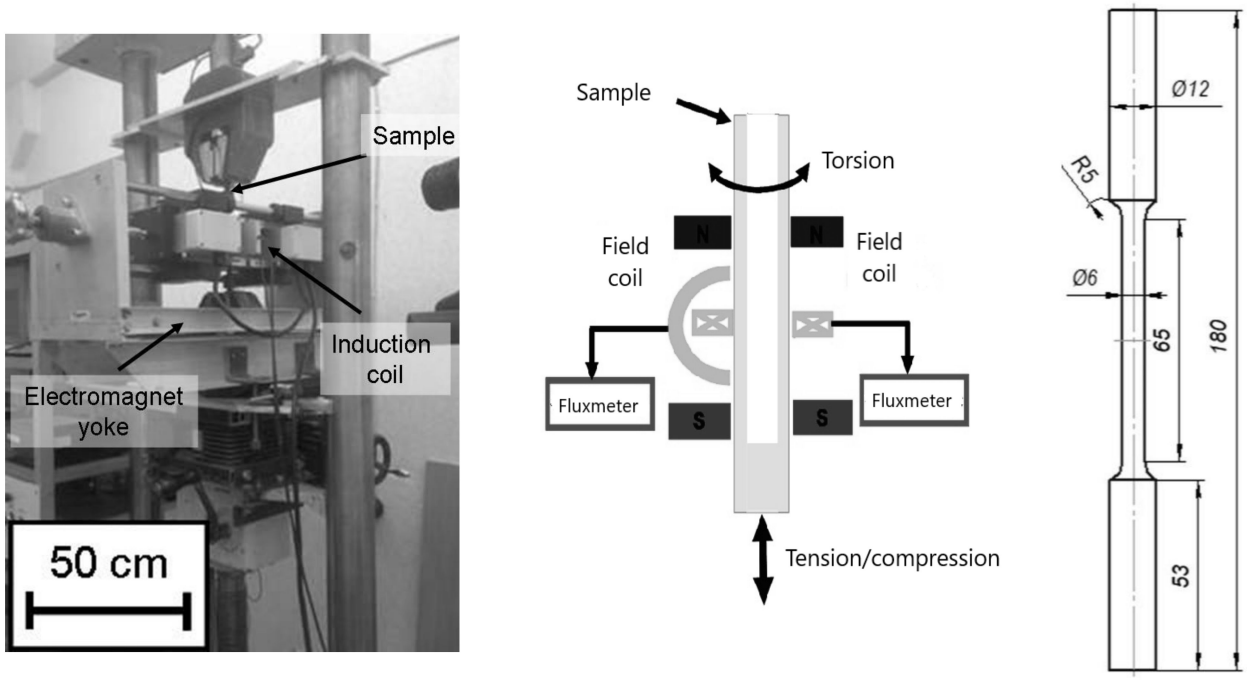

(**a**) (**b**) (**c**)

Figure 1. Appearance (**a**) and layout (**b**) of the installation for studying the effect of elastic–plastic deformation on the magnetic characteristics of materials, and the type of investigated sample (**c**) (all dimensions are in mm).

Deformation of the samples by tension and torsion was carried out with simultaneous recording of the magnetic hysteresis loops. Upon reaching a certain degree of deformation, the process of loading was stopped without load removal of the sample, and the magnetic hysteresis loops (MGL) were recorded by means of a Remagraph C-500 magnetic measuring complex. Magnetic measurements were carried out in a closed magnetic circuit according to the permeameter method. The strength of the magnetic field used during the experiment was up to 500 A/cm and was applied along the sample axis. The MGL were used to determine the values of the coercive force H_c, residual induction B_r, and magnetization in the maximum applied field M_{max} (approximately equal to the saturation magnetization). The error in measuring the field and induction did not exceed 3%. The maximum magnetic permeability μ_{max} was determined from the main magnetization curve.

The mechanical properties of the samples (yield strength σ_Y, ultimate strength σ_U, and relative elongation δ) were determined in accordance with GOST 1497-84 (State Standard of the former USSR). The stress–strain diagram of the investigated 13Cr-V steel is shown in Figure 2. The diagram reveals a tooth and a yield plateau typical of low-carbon steels.

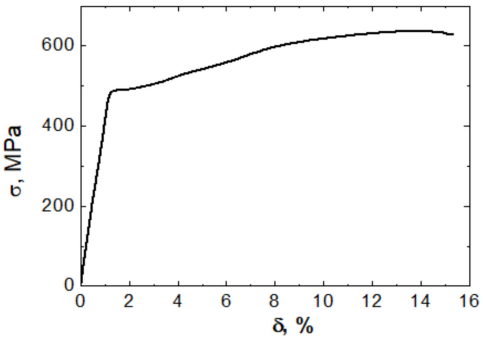

Figure 2. The stress–strain diagram of the investigated 13Cr-V steel. The curve originates from the tensile test in accordance with GOST 1497-84.

Tensile elongation of the samples was determined using the Strain Master non-contact strain measurement system (video extensometer) from LaVision.

The deformation degree of the samples at the *i*-th step of tensile deformation was determined as [23]:

$$\varepsilon_i = \ln(l_i/l_0), \tag{1}$$

where l_0 is the initial length of the working part of the sample and l_i is the length of the working part of the sample after the *i*-th loading step.

In the case of torsion, when the deformation over the cross section of the sample is unevenly distributed, the average value of the degree of deformation was calculated [24]:

$$\varepsilon_i^{\text{cp}} = \frac{2}{3}\varepsilon_i = \frac{2}{3} \cdot \frac{\varphi_i D}{2l_0\sqrt{3}} = \frac{\varphi_i D}{3l_0\sqrt{3}}, \tag{2}$$

where φ_i (rad) is the current twist angle of the sample and D = 6 mm is the diameter of the working part of the sample.

Microstructure studies were performed using an optical microscope, as well as a Tescan scanning electron microscope equipped with an Advanced AZtecHKL diffraction (EBSD) analysis system. For microstructural studies, a sample was cut in the initial state, as well as after deformation by tension and torsion. After tension and torsion, the sample for preparing a transverse section was cut at a distance of no more than 2 mm from the fracture zone (Figure 3). The section was subjected to grinding on diamond pastes and final polishing with a colloidal solution. The recording of diffraction patterns using the diffraction (EBSD) analysis system, both in tension and in torsion, was carried out in two places: in the center of the transverse section and closer to the surface.

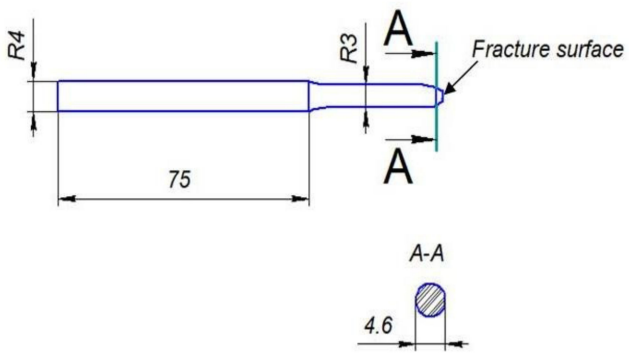

Figure 3. Scheme of sample cutting for the preparation of a thin section of the sample after fracturing for use in microscopic studies. This figure shows the example after the uniaxial tensile test. For torsion, the cutting method is similar (all dimensions are in mm).

3. Results and Discussion

3.1. Microstructure Investigation

In the initial state, the microstructure of 13Cr-V steel (Figure 4) is a mixture of ferrite, pearlite, and a small fraction of acicular bainite. The grain size of the metal is 8–15 microns. According to the recrystallization maps in the initial state, deformed grains were not identified in the sample structure (Figure 4c).

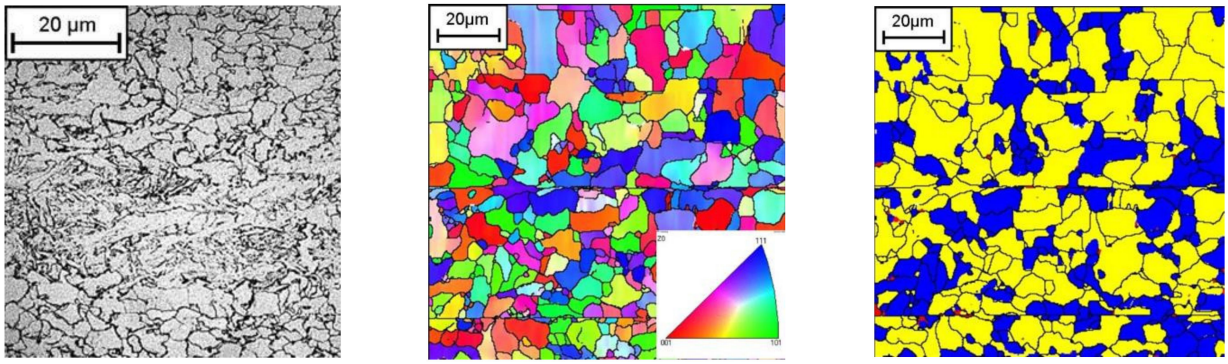

(**a**) (**b**) (**c**)

Figure 4. The microstructure of 13Cr-V steel in the initial state: (**a**) optical microstructure, (**b**) EBSD maps of misorientations, and (**c**) the map of recrystallization.

The mechanical properties of the investigated steel are given in Table 2. Tests to determine the mechanical characteristics were carried out according to GOST 1497-84 (the Russian standard) at room temperature during uniaxial tensile tests. Table 2 shows the results averaged over three samples; the error was no more than 5%. The table also shows the ratio of the yield strength to the tensile strength σ_Y/σ_B, which characterizes the material's work-hardening ability, usually specified by the normative documentation for the material. This indicator is often used in regulatory documentation for pipe products.

Table 2. The mechanical properties of the investigated steel.

Steel Grade	σ_Y, MPA	σ_U, MPa	σ_Y/σ_U	δ, %
13Cr-V	490 ± 25	640 ± 32	0.77	17 ± 1

From the point of view of mechanics, torsion is a softer deformation method than uniaxial tension. Under uniaxial tension, it is considered that the deformation of the working part of the sample occurs uniformly. Under torsion, the situation is different: the deformation over the sample cross section is distributed unevenly, with a maximum on the surface and a minimum in the center of the sample. Figure 5 shows EBSD maps of misorientations in the center of the cross sections of the studied steel after uniaxial tension (a) and torsion (b), prepared in the plane of the transverse axis of the sample. Since the section was prepared directly adjacent to the fracture zone in the region of neck formation, it can be assumed that the deformation in this place was practically the maximum for each type of test (uniaxial tension or torsion). In the central part of the samples, both after tension and after torsion, the microstructure consists of deformed (red color on recrystallization maps), but mostly form-unchanged, grains. Figure 6 demonstrates EBSD maps of misorientations near the surface of the cross sections of the studied steel after uniaxial tension (a) and torsion (b). It can be seen from the given figures that, under tension, the grains mostly retain their shape, i.e., remain close to the equiaxed form, although deformation and grinding occurs (Figures 5a and 6a). During torsion, it is clearly seen that the grains are deformed and stretched at a certain angle to the radial direction (Figure 6b), so the grains change their geometry. This is due to the fact that torsion deformation occurs

in a plane perpendicular to the axis of the sample, in contrast to tension, where the direction of deformation coincides with the axis of the sample. For a sample after torsion, texture formation is observed in the deformation plane, mainly in the <111> direction; it should be noted that along these crystallographic axes, iron and iron-based alloys have maximum strength [25].

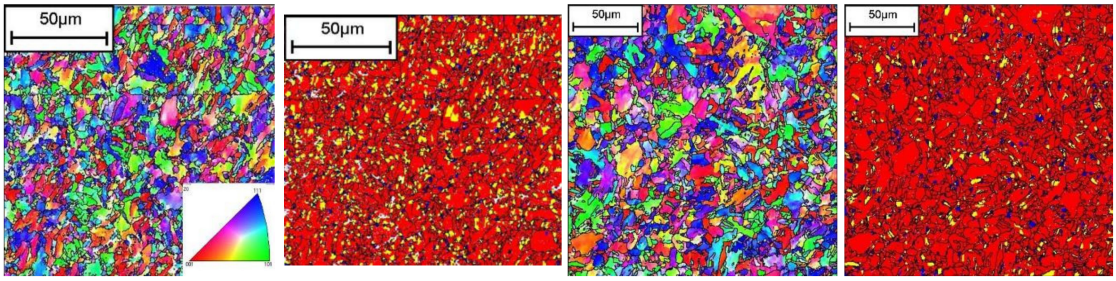

(**a**) (**b**)

Figure 5. EBSD maps of misorientations of the central sections of ruptured samples after uniaxial tension (**a**) and torsion (**b**), prepared in the plane of the transverse axis of the sample. The scheme of sample cutting used for these investigations is shown in Figure 3.

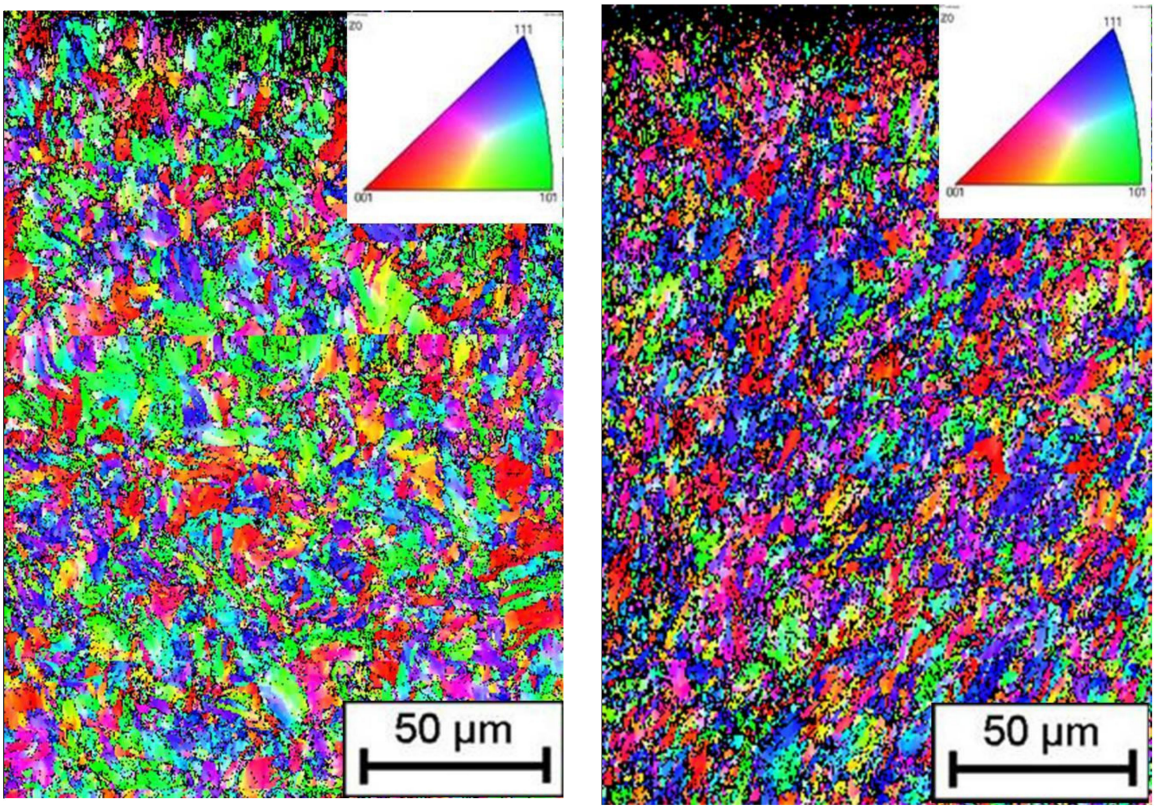

(**a**) (**b**)

Figure 6. EBSD maps of misorientations near the surface sections of ruptured samples after uniaxial tension (**a**) and torsion (**b**), prepared in the plane of the transverse axis of the sample. The scheme of sample cutting for these investigations is shown in Figure 3.

With an increase in the degree of plastic deformation, the density of dislocations in the sub-boundaries of the material increases and, as a result, crystallographic misorientations between subgrains grow, which leads to the transformation of sub-boundaries into ordinary high-angle grain boundaries [26]. As a result, a new, more dispersed deformed structure is

formed. Thus, we observe fragmentation of the structure during plastic deformation [27]. Moreover, similar mechanisms are applicable for uniaxial tension and torsion. After destruction of the sample near the destruction zone, the volume fraction of deformed grains after uniaxial tension was 93%, and after torsion, it was 87% (EBSD images were taken closer to the surface, because during torsion, the maximum deformation is observed in this region).

Figure 7 shows the histograms obtained by EBSD analysis, which describe the distribution of misorientations of elements of the subgrain structure of the samples after tension (a) and torsion (b). It can be seen that, in the initial state, the misorientation angle varies from 0 to 1.2°, with the average size being 0.5°. After uniaxial tension, the misorientation angle changes from 0.05° to 11.65°. In this case, the calculated average size of the misorientation angle inside the grain was 7.2°. During torsion, a slight shift in the misorientation angles of the subgrain structure towards larger angles occurs. Thus, the average size of the misorientation angle inside the grain was 8.2°. This fact confirms the association of deformation processes with a change in the level of distortions of crystallographic lattices of structural components.

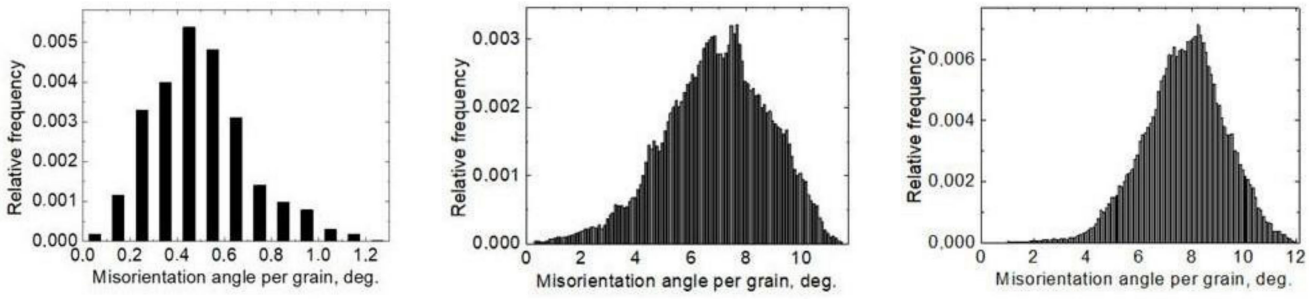

(**a**) (**b**) (**c**)

Figure 7. Angles of misorientation of elements of the subgrain structure of 13Cr-V steel samples in the initial state (**a**), after uniaxial tension (**b**) and after torsion (**c**). The studies were carried out on samples after the fracture in the plane of the transverse axis of the sample. The cutting scheme of the sample used for EBSD analysis is shown in Figure 3.

3.2. Investigation of Magnetic Properties

A change in the stress–strain state leads to a change in all types of energies in a ferromagnet, which, in turn, affects the course of magnetization and demagnetization processes in it [28]. Therefore, one of the objectives of the research is to determine a structure-sensitive parameter (or a combination of several parameters) that will change monotonically depending on the magnitude of the applied stresses. Figure 8 shows the dependences of the magnetic characteristics (the coercive force H_c, residual induction B_r, and the maximum magnetic permeability μ_{max}) on the applied normal and shear stresses of the studied steel.

A change in the structure under external action, in our case, deformation, is accompanied by a change in the energy state of the ferromagnetic material and, accordingly, its domain structure, which is reflected in the magnetic characteristics [29]. The action of elastic deformation is accompanied by the formation of a special domain structure (the so-called magnetic texture), which determines the processes of magnetization and magnetization reversal in a ferromagnet.

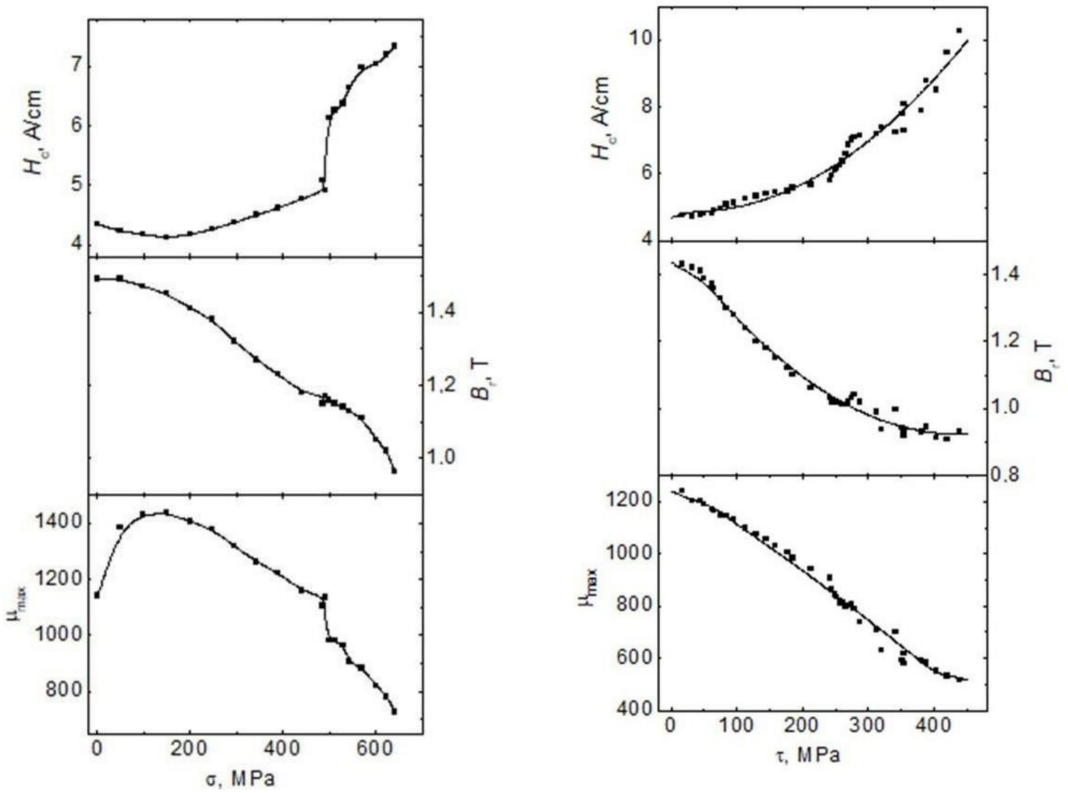

Figure 8. Dependences of magnetic parameters (coercive force H_c, residual induction B_r, and maximum magnetic permeability μ_{max}) on applied normal (tension) (**a**) and tangential (torsion) (**b**) stresses. The error in the determination of magnetic properties was no more than 3%.

The $H_c(\sigma)$ and $\mu_{max}(\sigma)$ dependences show an extremum in the region σ = 120–150 MPa (Figure 8a). These extrema in the elastic region of tension can be explained by the formation of a magnetic stress texture, also called induced magnetic anisotropy [30]. If the magnetostriction of the material and the external stresses are of the same sign, then the predominant orientation of the magnetic moments of the domains will be along the direction of application of the load, and, therefore, during magnetization along the tension axis, a decrease in the values of the coercive force and an increase in the maximum magnetic permeability (positive magnetoelastic effect) are observed. In this case, when the domain structure is rearranged, a preferential direction of the magnetization vectors of the "easy magnetization axis" type arises, and the processes of magnetization reversal in the direction of stress action are facilitated. However, upon further loading, the magnetostriction of iron and iron-based alloys can change sign [31,32], due to which the type of magnetic texture changes from the "easy magnetization axis" to the "easy magnetization plane", and the coercive force will increase and μ_{max} will decrease (negative magnetoelastic effect). The action of stresses reaching and exceeding the yield point leads to the destruction of the magnetic stress texture [30–32], and the main factor affecting the coercive force in the region of plastic deformation is an increase in the density of dislocations and dislocation clusters ($H_c \sim N^{1/2}$, where N is the dislocation density [33]).

It is also clearly seen in Figure 8a that in the transition from the elastic region of deformation to the region of developed plastic deformation, the coercive force and the maximum magnetic permeability change abruptly. This fact can be used to determine the conversion of a material under investigation from the elastic deformation region to the plastic deformation region.

In contrast to the coercive force and maximum magnetic permeability, the residual induction, depending on the applied uniaxial tensile stresses, varies unambiguously over the entire range of applied stresses. It was shown in [28] that some magnetic characteristics of more alloyed steels become monotonic over the entire range of elastic deformations. This allows us to say that residual induction may be the most suitable informative parameter for developing methods for diagnostic changes in the stress–strain state of details and elements made of 13Cr-V steel.

Figure 8b shows the change in the magnetic characteristics of 13Cr-V steel under the action of shear stresses. In our case, under the action of shear stresses, all the presented magnetic parameters change unambiguously over the entire range of applied shear stresses. This fact could be explained by the fact that during torsion, compared with the tension and the compression, two types of magnetic texture are simultaneously formed in the material [30]: 1—a type of "easy magnetization axis", which coincides with the direction of application of the load and facilitates magnetization along the sample axis; 2—a type of "easy magnetization plane", which is perpendicular to the sample axis and makes it difficult to magnetize along the sample axis. In earlier work, it was shown that tangential stresses have a weaker effect than normal stresses on the magnetic characteristics of constructional steels [22,34]. It was found in [28] that shear stresses arising during torsion are the same as a pair of normal, mutually perpendicular tensile and compressive stresses located at an angle of 45° to the sample axis.

In our case, all the studied characteristics (coercive force, residual induction, and maximum magnetic permeability) change unambiguously over the entire range of applied shear stresses during torsion. At the same time, it should be noted that in some earlier work [22,34], it was shown that the magnetic parameters are much less sensitive to changes in tangential loads than to normal loads. In this study concerning 13Cr-V steel, the sensitivity to the action of shear stresses is comparable to the sensitivity of the magnetic parameters to the action of normal stresses.

4. Conclusions

The effect of applied normal and shear stresses on the structure and magnetic parameters of low-carbon 13Cr-Vsteel pipe has been studied.

It is shown that torsion deformation leads to dispersion and the formation of elongated grains with a predominant crystallographic orientation in the structure near the surface, in contrast to the case of uniaxial tension, in which the grains are deformed uniformly, both in the center of the sample and near to the surface.

The presence of a sharp change in the level of coercive force and maximum magnetic permeability during the transition from the region of elastic deformation to the region of plastic deformation makes it possible to use them to indicate the conversion of a material from the elastic region of deformation to developed plastic deformation.

The residual induction changes unambiguously over the entire range of applied normal stresses, which makes it possible to use this parameter as information for developing methods for assessing the stress–strain state of products made of 13Cr-V steel during operation.

In the case of the action of shear stresses, coercive force, residual induction and maximum magnetic permeability, in view of the monotonicity of their change depending on the applied shear stresses, can be used later in the development of specific nondestructive testing methods for the objects made of the investigated steel.

At the same time, the sensitivity of the established magnetic parameters, both for the action of normal stresses and tangential stresses, is quite high.

Author Contributions: Conceptualization, E.P.; methodology, E.P.; investigation, K.K. and E.P.; data curation, K.K. and E.P.; visualization, K.K.; supervision, E.P.; project administration, E.P. All authors have read and agreed to the published version of the manuscript.

Funding: This study was supported by the Russian Science Foundation, project no. 20-79-00045.

Conflicts of Interest: The authors declare no conflict of interest.

References

1. Liu, M.; Fan, Y.; Gui, X.; Hu, J.; Wang, X.; Gao, G. Relationship between Microstructure and Properties of 1380 MPa Grade Bainitic Rail Steel Treated by Online Bainite-Based Quenching and Partitioning Concept. *Metals* **2022**, *12*, 330. [CrossRef]
2. Suetrong, C.; Uthaisangsuk, V. Investigations of fatigue crack propagation in ER8 railway wheel steel with varying microstructures. *Mater. Sci. Eng. A* **2022**, *18*, 142980. [CrossRef]
3. Ohaeri, E.G.; Szpunar, J.A. An overview on pipeline steel development for cold climate applications. *J. Pipeline Sci. Eng.* **2022**, *1*, 1–17. [CrossRef]
4. Efron, L.I. *Material Science in "Big" Metallurgy. Pipe Steels*; Metallurgizdat: Moscow, Russia, 2012; 696p.
5. Wang, H.; Ge, Y.; Shi, L. Technologies in deep and ultra-deep well drilling: Present status, challenges and future trend in the 13th Five-Year Plan period (2016–2020). *Nat. Gas Ind. B* **2017**, *4*, 319–326. [CrossRef]
6. Fan, Y.; Liu, T.G.; Xin, L.; Han, Y.M.; Lu, Y.H.; Shoji, T. Thermal aging behaviors of duplex stainless steels used in nuclear power plant: A review. *J. Nucl. Mater.* **2021**, *544*, 152693. [CrossRef]
7. Hizli, H.; Hakan, C. Applicability of the Magnetic Barkhausen Noise Method for Nondestructive Measurement of Residual Stresses in the Carburized and Tempered 19CrNi5H Steels. *Res. Nondestruct. Eval.* **2018**, *29*, 221–236. [CrossRef]
8. Kaijalainen, L.P.; Moilanen, M. Detection of plastic deformation during fatigue of mild steel by the measurements of Barkhausen noise. *NDT Int.* **1979**, *12*, 51–55. [CrossRef]
9. Vengrinovich, V.; Vintov, D.; Prudnikov, A.; Podugolnikov, P.; Ryabtsev, V. Magnetic Barkhausen Effect in Steel Under Biaxial Strain/Stress: Influence on Stress Measurement. *J. Nondestruct. Eval.* **2019**, *38*, 52. [CrossRef]
10. Mierczak, L.L.; Jiles, D.C.; Fantoni, G. A New Method for Evaluation of Mechanical Stress Using the Reciprocal Amplitude of Magnetic Barkhausen Noise. *IEEE Trans. Magn.* **2011**, *2*, 459–465. [CrossRef]
11. Schajer, G.S. *Practical Residual Stress Measurement Methods*; John Wiley & Sons Ltd.: Vancouver, BC, Canada, 2013. [CrossRef]
12. Chen, H.-E.; Xie, S.; Chen, Z.; Takagi, T.; Uchimoto, T.; Yoshihara, K. Quantitative Nondestructive Evaluation of Plastic Deformation in Carbon Steel Based on Electromagnetic Methods. *Mater. Trans.* **2014**, *55*, 1806–1815. [CrossRef]
13. Kurz, J.H.; Szielasko, K.; Tschuncky, R. Micromagnetic and Ultrasound Methods to Determine and Monitor Stress of Steel Structures. *J. Infrastruct. Syst.* **2017**, *2*, B4016009. [CrossRef]
14. Roskosz, M.; Fryczowski, K. Magnetic methods of characterization of active stresses in steel elements. *J. Magn. Magn. Mater.* **2020**, *499*, 166272. [CrossRef]
15. Qiu, F.; Ren, W.; Tian, G.Y.; Gao, B. Characterization of applied tensile stress using domain wall dynamic behavior of grain-oriented electrical steel. *J. Magn. Magn. Mater.* **2017**, *432*, 250–259. [CrossRef]
16. Takahashi, S.; Kobayashi, S.; Tomas, I.; Dupre, L.; Vertesy, G. Comparison of magnetic nondestructive methods applied for inspection of steel degradation. *NDT E Int.* **2017**, *91*, 54–60. [CrossRef]
17. Scherbinin, V.E.; Gorkunov, E.S. *Magnetic Quality Control of Metals*; UB RAS: Ekaterinburg, Russia, 1996; 263p.
18. Gorkunov, E.S.; MitropolskayaSYuVichuzhanin, D.I.; Tueva, E.A. Magnetic methods for estimation of loading and damaging in X70 steel. *Phys. Mesomech.* **2010**, *1*, 73–82.
19. Mészáros, I.; Szabó, P.J. Complex magnetic and microstructural investigation of duplex stainless steel. *NDT E Int.* **2005**, *7*, 517–521. [CrossRef]
20. Gorkunov, E.S.; Zadvorkin, S.M.; Kokovikhin, E.A.; Tueva, E.A.; Subachev, Y.u.V.; Goruleva, L.S.; Podkopytova, A.V. The effects of deformations by rolling and uniaxial tension on the structure and the magnetic and mechanical properties of armco iron, steel 12Cr1Nih10Ti, and a steel 12Cr1Nih10Ti-armco iron-steel 12Cr1Nih10Ti composite material. *Russ. J. Nondestruct. Test.* **2011**, *6*, 369–380. [CrossRef]
21. Oršulová, T.; Palček, P.; Roszak, M.; Uhríčik, M.; Smetana, M.; Kúdelčík, J. Change of magnetic properties in austenitic stainless steels due to plastic deformation. *Procedia Struct. Integr.* **2018**, *13*, 1689–1694. [CrossRef]
22. Gorkunov, E.S.; Putilova, E.A.; Zadvorkin, S.M.; Makarov, A.V.; Pecherkina, N.L.; Kalinin, G.Y.; Mushnikova, S.Y.; Fomina, O.V. Behavior of magnetic characteristics in promising nitrogen-containing steels upon elastoplastic deformation. *Phys. Met. Metallogr.* **2015**, *8*, 838–849. [CrossRef]
23. Smirnov, S.V.; Shveikin, V.P. *Plasticity and Deformability of Carbon Steels during Pressure Treatment*; UB RAS: Ekaterinburg, Russia, 2009; 254p.
24. Kolmogorov, V.L. *Stress, Deformation, Destruction*; Metallurgy: Moscow, Russia, 1970; 230p.
25. Anastasiady, G.P.; Sil'nikov, M.V. *Heterogeneity and Performance of Steel*; Poligon: Saint Petersburg, Russia, 2002; 624p.
26. Rybin, V.V. *Large Plastic Deformations and Destruction of Metals*; Metallurgia: Moscow, Russia, 1986; 224p.
27. Zolotorevsky, N.Y.; Rybin, V.V. *Fragmentation and Texture Formation during Deformation of Metallic Materials*; Polytechnic University Press: Saint Petersburg, Russia, 2014; 207p.
28. Gorkunov, E.S.; Mushnikov, A.N. Magnetic methods of evaluating elastic stresses in ferromagnetic steels (review). *Test. Diagn.* **2020**, *12*, 4–23. [CrossRef]
29. Gorkunov, E.S. Influence of heat treatment on magnetostriction of structural steel 34Khn2M. *Defektoskopiya* **1979**, *11*, 105–108.
30. Vonsovsky, S.V.; Schur, Y.S. *Ferromagnetizm*; OGIZ: Saint Petersburg, Russia, 1948; 816p.
31. Dunaev, F.N. On the magnetic texture of elastically stretched transformer steel. *Izv. Vuzov Phys. Ser.* **1962**, *1*, 151–153.

32. Zaykova, V.A.; Schur, Y.S. On the effect of tension on the magnetic properties and magnetostriction curves of silicon iron. *Phys. Met. Metallogr.* **1966**, *5*, 664–673.
33. Kersten, M. *Die Bedeutung der Koerzitivkraft. Probleme der Technischen Magnetisierungskurve*; Becker, R., Ed.; Springer: Berlin, Germany, 1938; pp. 42–72.
34. Gorkunov, E.S.; Zadvorkin, S.M.; Putilova, E.A.; Savrai, R.A. Effect of the Structure and Stress State on the Magnetic Properties of Metal in Different Zones of Welded Pipes of Large Diameter. *Phys. Met. Metallogr.* **2014**, *10*, 1011–1018. [CrossRef]